Time- and Voltage-Dependent Components of Kv4.3 Inactivation

Shimin Wang,*† Vladimir E. Bondarenko,* Yu-jie Qu,* Glenna C. L. Bett,* Michael J. Morales,* Randall L. Rasmusson,* and Harold C. Strauss*

*Department of Physiology and Biophysics, University at Buffalo, The State University of New York, School of Medicine and Biomedical Sciences, Buffalo, New York; and †Department of Cardiology, Renmin Hospital of Wuhan University, Wuhan, Hubei, China

ABSTRACT Kv4.3 inactivation is a complex multiexponential process, which can occur from both closed and open states. The fast component of inactivation is modulated by the N-terminus, but the mechanisms mediating the other components of inactivation are controversial. We studied inactivation of Kv4.3 expressed in *Xenopus laevis* oocytes, using the two-electrode voltage-clamp technique. Inactivation during 2000 ms pulses at potentials positive to the activation threshold was described by three exponents (46 ± 3, 152 ± 13, and 930 ± 50 ms at +50 mV, $n = 7$) whereas closed-state inactivation (at potentials below threshold) was described by two exponents (1079 ± 119 and 3719 ± 307 ms at −40 mV, $n = 9$). The fast component of open-state inactivation was dominant at potentials positive to −20 mV. Negative to −30 mV, the intermediate and slow components dominated inactivation. Inactivation properties were dependent on pulse duration. Recovery from inactivation was strongly dependent on voltage and pulse duration. We developed an 11-state Markov model of Kv4.3 gating that incorporated a direct transition from the open-inactivated state to the closed-inactivated state. Simulations with this model reproduced open- and closed-state inactivation, isochronal inactivation relationships, and reopening currents. Our data suggest that inactivation can proceed primarily from the open state and that multiple inactivation components can be identified.

INTRODUCTION

The rapidly inactivating, voltage-dependent K^+ channels in neurons, and cardiac and smooth muscle myocytes have received much attention recently (1–9). In heart, the rapidly inactivating K^+ current (I_{to}) plays an important role because it makes a major contribution to the early and subsequent stages of repolarization, and as a result to excitation-contraction coupling (1,10,11). Among the different candidate clones that have been proposed to serve as molecular substrates for this current are the pore-forming α-subunits, Kv4.2 and/or Kv4.3 in the heart of many animal species and humans (12–17). Despite these advances in our understanding of channel function and composition, the mechanism of Kv4.3 inactivation is still incompletely resolved.

Kv4 channels continue to attract great interest because their mechanism of gating differs significantly from that reported for *Shaker* and Kv1.4 channels (3,6,18–22). In *Shaker* and Kv1.4 channels, inactivation is governed by N- and C-type inactivation attributed to a ball and chain mechanism occluding the inner vestibule (N-type), and external and internal pore closure (C-type) (19,23–27). In contrast, in Kv4 inactivation is more complex. Deletion of the amphipathic region of the N-terminus of Kv4.1 abolishes the first or rapid component of inactivation; however, deletions in the largely hydrophilic (mostly basic) domain in the C-terminus also abolish the rapid component of inactivation. On the other hand, when a Kv4.2 N-terminal deleted mutant is expressed, the fast component of inactivation is restored by the application of a synthetic peptide corresponding to the deleted Kv4.2 N-terminus to the cytoplasmic side of the membrane (6). In addition, the slower components of inactivation in Kv4 differ from C-type inactivation reported for *Shaker* K^+ channels. For example, in Kv4.1 and Kv4.3, elevated $[K^+]_o$ accelerates inactivation, whereas it has little effect on Kv1.4 inactivation time course (18,20,28). On the other hand, recovery from inactivation was slowed in Kv4.1, but accelerated in Kv1.4. TEA, an open channel blocker of *Shaker* channels, that has been shown to compete with N-type and C-type inactivation, when applied internally and externally, respectively, has little effect on the gating kinetics of Kv4.1 (20,25,26). Finally, in contrast to *Shaker* K^+ channels, there appears to be a substantial degree of inactivation in the Kv4 family that occurs from a preopen closed state (3,21,22). Hence, inactivation gating in Kv4 appears to be much more complex than in *Shaker* K^+ channels.

Although prior studies have advanced our understanding of inactivation in Kv4, a substantial number of issues have not been addressed. Experiments performed on Kv4 gating by Jerng et al. (21), Bähring et al. (22), and Beck et al. (3) indicated that the time course of Kv4 inactivation is described by two or three exponents. In a series of models developed for Kv4.2 and Kv4.3, channel inactivation occurred from both open and closed states, where the open to inactive state transition was nonabsorbing and the closed to open transition was reverse biased, resulting in an unstable open-inactivated state (3). However, whereas the Kv4.3 model is widely accepted (5,7,9), it has several shortcomings that made us reexamine Kv4.3 inactivation and develop a new model of inactivation. Inactivation gating in channels with conventional N- and C-type mechanisms (*Shaker* and

Submitted January 11, 2005, and accepted for publication July 15, 2005.

Address reprint requests to Dr. Harold C. Strauss, Dept. of Physiology and Biophysics, University at Buffalo, The State University of New York, School of Medicine and Biomedical Sciences, 124 Sherman Hall, 3435 Main St., Buffalo, NY 14214. Tel.: 716-829-2738; Fax: 716-829-2344; E-mail: hstrauss@buffalo.edu.

0006-3495/05/11/3026/16 $2.00

doi: 10.1529/biophysj.105.059378

Kv1 channels) revealed that N- and C-type inactivation has the same coupling to the activation process (18). In contrast, in Kv4 channels the different inactivation states are coupled to different states in the activation pathway (3,22). This implies that the differences in time- and voltage-dependent properties can be used to elucidate inactivation mechanisms. Furthermore, the existence of different coupling mechanisms makes the testable prediction that these mechanisms will not only have different properties of inactivation at particular potentials, but may also possess different properties of recovery. Thus, the objective of this study was to elucidate experimentally the time- and voltage-dependent properties of the complex inactivation and recovery processes and their potential coupling to different stages of activation.

In this article, we show that the inactivation properties of Kv4.3 are more complex than previously described. We found that inactivation kinetics are markedly different for closed- and open-state inactivation and are voltage dependent. The kinetics of recovery from inactivation are strongly voltage dependent and depend on pulse duration. This suggests that the recovery process involves energetic coupling to the backward movement of the voltage sensor. Using short, intermediate, and long pulses, we were able to resolve different ''quasi-steady-state'' or isochronal inactivation relationships. Differences in the isochronal inactivation relationships and recovery kinetics enabled us to discriminate between these distinct inactivation pathways. Such isochronal inactivation relationships cannot be simulated by the previously published gating model of Kv4.3 (3). Our data argue against the view that Kv4.3 inactivation occurs predominantly from the closed state. As a result, we developed a model of Kv4.3 gating that incorporates inactivation from both closed and open states and does not exclude direct communication between the open-inactivated and closed-inactivated states.

MATERIALS AND METHODS

cRNA preparation and channel expressions

Rat wild type (WT) cDNA of Kv4.3 (short form), a gift of Dr. David McKinnon (Stony Brook, SUNY) was utilized in these studies. The construct of rat Kv4.3 has been previously described (29).

Mature female *Xenopus laevis* (*Xenopus* One, Ann Arbor, MI) were anesthetized by immersion in a solution of ethyl 3-aminobenzoate methane sulfonate salt (Sigma Aldrich, St. Louis, MO) (1.5 g l^{-1}). Ovarian lobes were removed through a small incision in the abdominal wall. After removal of the ovarian lobe, the incisions were sutured closed and the frogs were then allowed to recover in a small water-filled container as previously described (30). Typically, lobes were obtained three times from a single frog. When individual frogs no longer yielded acceptable oocytes, anaesthetized frogs were killed by an overdose of ethyl 3-aminobenzoate methane sulfonate salt (30 g l^{-1}).

The lobes were placed in a collagenase-containing, Ca^{2+}-free OR2 solution ((in millimolar) 82.5 NaCl, 2 KCl, 1 $MgCl_2$, 5 HEPES, pH 7.4; 1–2 mg ml^{-1} collagenase (Type II, Sigma Aldrich)) to remove the follicular layer. The solution containing the oocytes was gently agitated for ~2 h and collagenase activity was then arrested by bovine albumin as previously described (30). Defolliculated oocytes (stage V–VI) were then injected with transcribed cRNA (up to 50 nl) using a ''Nanoject'' microinjection system (Drummond Scientific, Broomall, PA) and incubated at 18°C for 24–72 h in an antibiotic-containing Barth's solution (in millimolar) 88 NaCl, 1 KCl, 2.4 $NaHCO_3$, 0.82 $MgSO_4$, 0.33 $Ca(NO_3)_2$, 0.41 $CaCl_2$, 10 HEPES (pH 7.4), 2% (v/v of 100 × stock) antibiotic-antimycotic (Gibco catalog No. 600-5240PG, Invitrogen, Carlsbad, CA).

Electrophysiological techniques

Oocytes were clamped using a two-microelectrode ''bath clamp'' amplifier (OC-750A, Warner Instruments, Hamden, CT), as had been described in detail elsewhere (30). Microelectrodes were fabricated from 1.5 mm o.d. borosillicate glass tubing (TW150F-4, WPI) using a two-stage puller (L/M-3 P-A, Adams & List Associates, Great Neck, NY) filled with 3 M KCl with resistances of 0.6–1.5 MΩ. During recording, oocytes were continuously perfused with control ND 96 solution (in millimolar) 96 NaCl, 2 KCl, 1 $MgCl_2$, 1.8 $CaCl_2$, 10 HEPES, pH 7.4, adjusted with NaOH or ND 98 solution (in millimolar) 98 KCl, 1 $MgCl_2$, 1.8 $CaCl_2$, 10 HEPES, pH 7.4, adjusted with NaOH. Currents were recorded at room temperature (21–23°C) and were filtered at 2.5 kHz.

Data analysis

Data were digitized, stored in a computer, and subsequently analyzed directly using pCLAMP 9 software (Axon Instruments, Foster City, CA). Unless otherwise stated, raw data traces from two-microelectrode voltage-clamp recordings were not leakage or capacitance subtracted. The pulse protocols and the equations that best fit the data are presented in each figure legend. Data are shown as mean ± SE. Confidence levels were calculated using Student's paired *t*-test.

The time course of both open- and closed-state inactivation were determined by fitting inactivation traces with the function, $f(t) = \Sigma_{j=1}^{N} A_j \exp(-t/\tau_j)$, where $N = 1$, 2, or 3 and A_j is the amplitude of jth component of inactivation, $j = 1$, 2, or 3. The kinetics of recovery from inactivation were determined by fitting recovery of the normalized peak current by the function, $f_{rec}(t) = 1 - \Sigma_{j=1}^{N} B_j \exp(-t/\tau_{recj})$, where $N = 1$ or 2 and B_j is the amplitude of jth component of recovery from inactivation, $j = 1, 2$. Steady-state inactivation was determined using a fitting function, $f_i(V) = f_{i0}/\{1 + \exp[(V - V_{1/2})/k]\} + (1 - f_{i0}) = f_{i0}/\{1 + \exp[-z_i e_0 (V - V_{1/2})/k_B T]\} + (1 - f_{i0})$, where f_{i0} is the constant, $V_{1/2}$ is the half-inactivation potential, k is the slope, z_i is the effective charge of the relationship, k_B is the Boltzmann constant, T is the absolute temperature, and e_0 is the elementary charge.

We estimated the effective charge from Kv4.3 gating properties. The effective charge represents the net charge movement across the membrane within an electric field. It depends on the magnitude and distance of charge movement (31). To determine the effective charge, one analyzes the voltage dependence of gating characteristics. However, any such analysis of inactivation and recovery from inactivation is model dependent, and in the case of steady-state inactivation the determination of effective charge is predicated on the transition from one steady state to another. For example, in the case of the analysis of steady-state inactivation different pulse durations were employed and different relationships were obtained. However, these relationships may have been obtained from transitions that did not reach steady-state conditions. Hence, we will term this condition as ''isochronal''. In addition, the estimate of effective charge under these conditions can be considered to be a qualitative rather than a quantitative measure of net charge movement, and as a result, the charge movement values are termed ''apparent effective charge''. We are also estimating apparent effective charge from gating transitions, which are reflected in gating properties (voltage dependence of inactivation kinetics, isochronal inactivation, and recovery from inactivation) and which are coupled to activation (see Appendix for further discussion).

Apparent effective charge of inactivation was calculated from a biexponential fit of the voltage dependence of inactivation time constants $\tau_j(V) = C_{1j} \exp(-V/V_{1j}) + C_{2j} \exp(-V/V_{2j})$, where C_{1j} and C_{2j} are the amplitudes of these exponential functions and V_{1j} and V_{2j} are the corresponding characteristic voltages, where $j = 1$, 2, or 3 for each component of inactivation. Apparent effective charge of recovery from inactivation was obtained from exponential fit of the voltage dependence of recovery time

constant $\tau_{recj}(V) = D_j \exp(-V/V_{recj})$, where D_j is the amplitude of this exponential function and V_{recj} is the corresponding characteristic voltage, $j = 1$ or 2. Apparent effective charges for time constants of inactivation and recovery from inactivation were determined from equations $z_x = k_BT/e_0V_x$, where $x = 1j$ or $x = 2j$ ($j = 1$, 2, or 3) for inactivation, $x = rec1$ or $x = rec2$ for recovery from inactivation. For isochronal inactivation, the apparent effective charge was calculated from the equation $z_i = k_BT/e_0k$, where k is the slope factor for $f_i(V)$. A theoretical basis for these estimates is given in the Appendix.

Gating model and simulation

Our model of inactivation was developed using Mathematica software (Wolfram Research, Champaign, IL) and it incorporated a previously published activation model of Kv4.3 (32). The model includes five closed states (C_0–C_4), one open state (O), and five inactivated states (I_f, I_i, I_s, I_{C3}, I_{C4}) (Scheme 2). We assumed that initially, at a resting potential of −90 mV, all channels were in the state C_0 ($C_0 = 1.0$), and all other states were empty. Rate constants were adjusted to fit our experimental data on Kv4.3 gating.

RESULTS

Previous experiments have established that inactivation can proceed both from the open state as well as the closed state (3,8,21,22). There is a consensus that open-state inactivation in Kv4.3 has at least two components, but widely different estimates of the kinetics of open- and closed-state inactivation in Kv4 channels have been reported (3,8,21,22). In previously published models (3,22), after opening, Kv4.3 transiently occupies open-inactivated states, then transits backward to the open state, and subsequently accumulates in the closed-inactivated state (Scheme 1). A direct transition from the open-inactivated state to a closed-inactivated state was not evaluated. The absence of formal consideration of additional gating models has limited our understanding of inactivation mechanisms. Specifically, do the different kinetic components of inactivation represent different mechanisms? Can the open-inactivated states communicate directly with the closed-inactivated states? To address these issues, we investigated the kinetics and isochronal properties of open- and closed-state inactivation and developed a model of Kv4.3 gating that allows for direct transitions between the final open-inactive and closed-inactive states. This new model closely simulates our inactivation data.

Open-state inactivation kinetics

To reconcile the apparent discrepancy in inactivation kinetics, we analyzed the kinetics of inactivation using depolarization pulses with different durations (500, 1000, and 2000 ms). We found that our ability to resolve the kinetics of inactivation was dependent on pulse duration. For pulses of 500 and 1000 ms duration, inactivation was well described by two exponents, whereas for 2000 ms pulses, inactivation was well described by three exponents. For 2000 ms pulses, the time constants of the three components of inactivation were 46 ± 3, 152 ± 13, and 930 ± 50 ms, respectively, at +50 mV (Fig. 1, *A* and *C*). Because the third (slow) component could only be identified with 2000 ms pulses, unless otherwise specified, all subsequent analyses of inactivation were performed using 2000 ms pulses to ensure that slow inactivation was nearly complete.

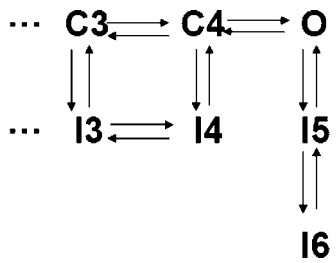

SCHEME 1

The time constants of open-state inactivation were voltage dependent and this voltage dependence of each component could be described by a biexponential function (Fig. 1 *C*). The fast component of open-state inactivation is likely to be coupled to the last voltage-independent step of the activation process (see Discussion) and as a result it would be of interest to calculate the apparent effective charge from the voltage dependence of the time course of inactivation. Apparent effective charge is used in this manuscript to enable us to combine and compare the steepness of voltage dependence of various kinetic and isochronal measurements of Kv4.3 gating across various conditions. The apparent effective charges for the fast component of inactivation were 2.28 e_0 and 0.58 e_0. The first value for apparent effective charge closely approximates the value of apparent effective charge for activation, 2.11 e_0 (32) and suggests that the fast component is coupled to the last step of the activation process (see Discussion; Table 1).

Our premise is that the different inactivation states have different kinetics and voltage dependence of recovery from inactivation. To further investigate whether the three components of open-state inactivation reflect three different pathways, we used short (67 ms) and long (800 ms) depolarizing pulses to inactivate the channel and compared the recovery from inactivation for these two cases (Fig. 2). Between −60 and −90 mV, significant differences in recovery times were observed. For example, at −90 mV, the time constant for recovery from inactivation (τ_{rec}) was 179 ± 17 and 240 ± 6 ms ($p < 0.02$; $n = 5$) for short and long pulses, respectively (Table 2). Estimation of the apparent effective charge from voltage dependence of recovery kinetics yields 0.77 e_0 and 0.94 e_0, for short and long pulses, respectively. These differences in τ_{rec} also provide additional support for the existence of multiple functionally distinct inactivated states for Kv4.3. At −120 and −90 mV, the recovery for both short and long pulses was monoexponential, whereas at voltages of −70 and −60 mV it was biexponential (Table 2; Figs. 2, *A* and *B*, and 3). Although the interpretation in terms of valence must be viewed with caution, our data demonstrate that multiple inactivated states can be at least partially separated kinetically through the recovery measurements. These data support the hypothesis that different components of inactivation

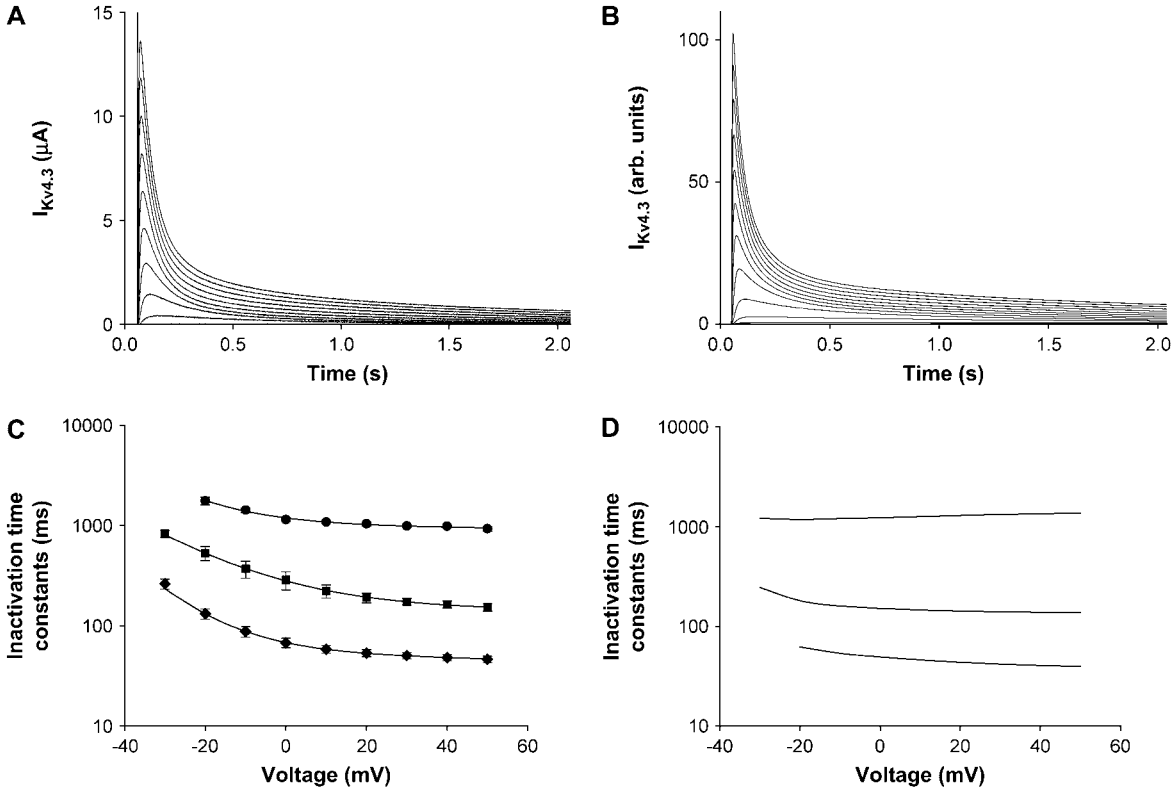

FIGURE 1 Time course of inactivation of Kv4.3 expressed in *Xenopus* oocytes. Experimental current traces from two-electrode voltage clamp (*A*) and inactivation time constants (*C*) of $I_{Kv4.3}$ during 2000 ms depolarization pulse. A range of voltage steps from the holding potential −90 mV were applied from −120 to +50 mV in 10 mV steps. Fitting function for analysis of inactivation is $f(t) = \Sigma_{j=1}^{N} A_j \exp(-t/\tau_j)$, where $N = 2$ and 3. Values for the fast, intermediate, and slow components of inactivation are shown by diamonds, squares, and circles, respectively. The solid lines in panel *C* represent fits of the experimental data. The kinetics of open-state inactivation were voltage dependent and this voltage dependence can be described by a biexponential function, with the apparent effective charge of 2.28 e_0 and 0.58 e_0 for the fast component, 1.63 e_0 and 1.04 e_0 for the intermediate component, and 1.73 e_0 and 0.16 e_0 for the slow component (*C*). In panel *C* at −30 mV the current was too small to allow fitting with three exponential functions. Data for inactivation time constants were obtained from seven cells. Panels *B* and *D* show computer simulations of current traces and inactivation time constants, respectively, using the model depicted in Scheme 2 and the transition rates shown in Table 3.

are coupled differently to the movement of the channel during activation.

Closed-state inactivation kinetics

To evaluate the kinetics of closed-state inactivation, we used subthreshold depolarizing pulses, using the protocol described by Beck and Covarrubias (33) (Fig. 4). These protocols consisted of four pulses, the first, P1, from −100 to +40 mV (800 ms); the second, P2, to −100 mV (5 s); the third, P3, to variable voltages and durations (voltage from −80 to −40 mV and duration from 800 ms to 14.4 s), and the fourth, P4, to +40 mV (800 ms) followed by a return to holding potential of −100 mV. The magnitude of P4 was used to measure the degree of inactivation that developed during P3. Closed-state inactivation was biexponential at −40 mV and monoexponential at −50 and −60 mV (Fig. 4 *B*). The slow time constant of inactivation varied from 3.7 ± 0.3 to 8.8 ± 1.4 s as P3 changed from −40 to −60 mV.

TABLE 1 Apparent effective charge for different gating processes in Kv4.3

	Apparent effective charge
Open-state isochronal inactivation	
Pulse duration, 67 ms (short)	2.48 e_0
Pulse duration, 150 ms (intermediate)	3.27 e_0
Pulse duration, 2000 ms (long)	4.72 e_0
Closed-state steady-state inactivation	6.54 e_0
Recovery from open-state inactivation	
Pulse duration, 67 ms (short)	0.77 e_0
Pulse duration, 800 ms (long)	0.94 e_0
Recovery from closed-state inactivation	1.20 e_0
Deactivation	0.48 e_0

Recovery from closed-state inactivation was monoexponential at voltages negative to −90 mV and biexponential at the voltages of −80 and −70 mV (Figs. 5 and 6). Estimation of effective charge from voltage dependence of recovery kinetics yields an apparent effective charge of 1.20 e_0, which is larger than the corresponding values for recovery from open-state inactivation using short and long pulses, 0.77 e_0 and 0.94 e_0, respectively (Table 1). These data provide

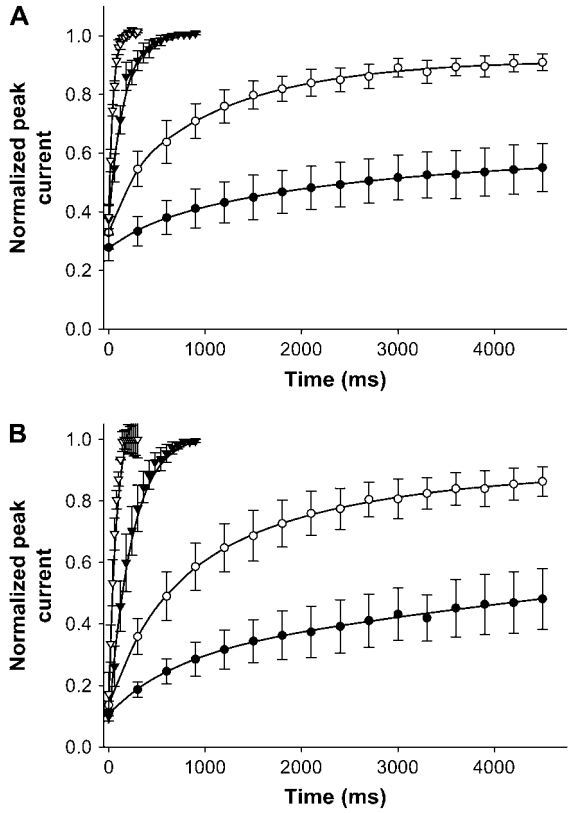

FIGURE 2 Recovery from inactivation. Normalized peak current values as a function of interpulse interval and holding potential (*A* and *B*) of $I_{Kv4.3}$. Either (*A*) 67 or (*B*) 800 ms pulses to +50 mV (P1) from the holding potential −90 mV were followed by the second 100 ms depolarization (P2) to +50 mV with variable time gap and interpulse holding potentials. The experimental data for interpulse holding potential of −120, −90, −70, and −60 mV are represented as ▽, ▼, ○, and ●, respectively. In panels *A* and *B*, data are expressed as means ± SE ($n = 3$). Solid lines represent fits to the experimental data.

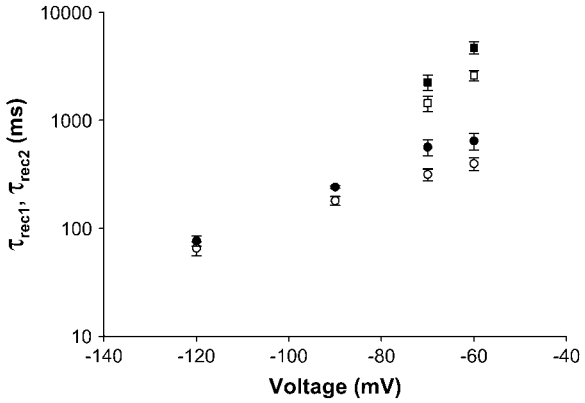

FIGURE 3 Kinetics of recovery from inactivation for short (67 ms, *open symbols*) and long (800 ms, *solid symbols*) P1 pulses. The time constants of recovery from inactivation were plotted as functions of interpulse holding potential. Recovery was monoexponential at −120 and −90 mV and biexponential at −70 and −60 mV. The fast and slow components of recovery from inactivation are plotted by circles and squares, respectively. Voltage-clamp protocols as described in Fig. 2. Data are expressed as means ± SE ($n = 5$).

additional support for the view that the closed-inactive state is different from the open-inactive state.

Isochronal inactivation

To assess further the different mechanisms of Kv4.3 inactivation, we measured isochronal open-state inactivation with short (67 ms), intermediate (150 ms), and long (2000 ms) pulses (Fig. 7). To evaluate the fast inactivation pathway ($\tau_1 = 46 \pm 3$ ms, +50 mV, 2000-ms pulse) we used a 67 ms pulse. However, a 67 ms pulse was too brief to allow the first component of open-state inactivation to reach steady state. The 150 ms pulse was sufficiently long to allow for near completion of fast open-state inactivation and partial inactivation via the second component ($\tau_2 = 152 \pm 13$ ms, +50 mV, 2000 ms pulse). The 2000 ms pulse allowed for complete inactivation via the fast and intermediate components and partial completion via the slow component ($\tau_3 = 930 \pm 50$ ms, +50 mV, 2000 ms pulse). In these three cases, significant differences in $V_{1/2}$ and k for isochronal inactivation relationships were observed; for the short pulse $V_{1/2} = -13.9$ mV and $k = 10.3$ mV ($n = 5$), for the intermediate pulse $V_{1/2} = -21.6$ mV and $k = 7.8$ mV ($n = 6$), and for the long pulse $V_{1/2} = -43.4$ mV and $k = 5.4$ mV ($n = 7$) (Fig. 7 *C*). The large differences in values of $V_{1/2}$ and k suggest that Kv4.3 has more than one inactivation pathway (see ''Markov model and simulations of Kv4.3 inactivation'' and Discussion). In addition, these data suggest that the apparent effective charge of inactivation is surprisingly dependent on pulse duration (2.48 e_0, 3.27 e_0, and 4.72 e_0, for short, intermediate, and long pulse durations, respectively). Hence, the differences in values of the $V_{1/2}$ and k for the three isochronal inactivation relationships could represent the different contributions of three components of inactivation.

TABLE 2 Effects of pulse duration on experimental kinetics of recovery from inactivation

Voltage	Pulse duration (67 ms) Fast component	Pulse duration (67 ms) Slow component	Pulse duration (800 ms) Fast component	Pulse duration (800 ms) Slow component
−120 mV	66 ± 10 ms	Undetermined	77 ± 9 ms	Undetermined
−90 mV	179 ± 17 ms	Undetermined	240 ± 6 ms	Undetermined
−70 mV	314 ± 39 ms	1438 ± 229 ms	563 ± 95 ms	2244 ± 364 ms
−60 mV	396 ± 53 ms	2601 ± 281 ms	643 ± 116 ms	4713 ± 623 ms

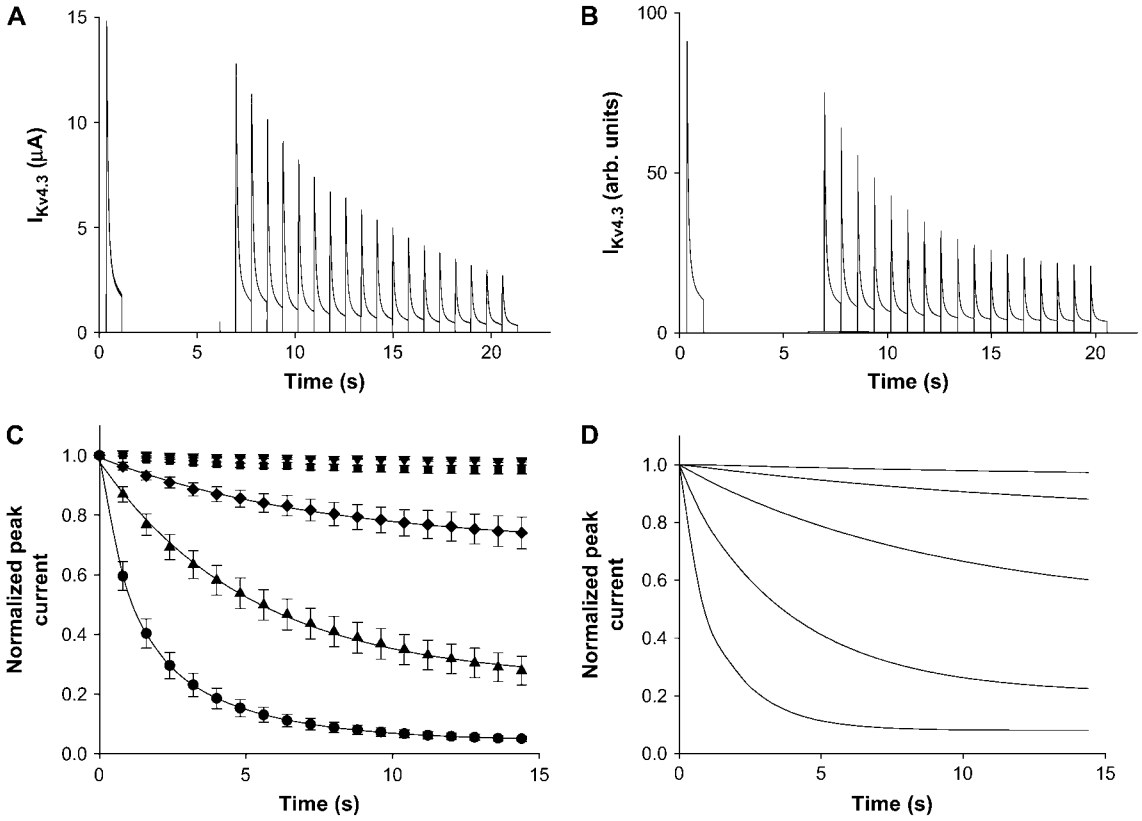

FIGURE 4 Voltage dependence of closed-state inactivation of $I_{Kv4.3}$. Voltage-clamp protocol consisted of four pulses: holding potential was −100 mV, first pulse (P1) amplitude was +40 mV and duration 800 ms, second pulse (P2) was set at −100 mV for 5000 ms, third pulse (P3) amplitude was varied from −80 to −50 mV and duration changed from 800 to 14,400 ms, and the fourth pulse (P4) amplitude was set at +40 mV for 800 ms. Panel *A* shows currents elicited at different times during P3 (−50 mV). Normalized current is plotted in panel *C* as function of pulse duration at different test potentials: −80 (▼), −70 (■), −60 (♦), −50 (▲), and −40 mV (●). Solid lines represent monoexponential fits for test potentials −60 and −50 mV and biexponential fits for the test potential of −40 mV. Number of cells in each experiment was $n = 9$. Panels *B* and *D* show simulated corresponding current traces (*B*) and normalized current plotted as a function of P3 duration (*D*).

Steady-state closed-state inactivation relationship is shown in Fig. 7 *C* ($V_{1/2} = -58.7$ mV and $k = 3.9$ mV). The value of $V_{1/2}$ for closed-state steady-state inactivation is more negative than for open-state isochronal inactivation obtained with short, intermediate, and long depolarization pulses. In addition, the slope, k, for closed-state steady-state inactivation relationship is steeper than for open-state isochronal inactivation relationships. These data suggest that the mechanisms of open- and closed-state inactivation differ.

Amplitudes of different components of inactivation

To understand further the contributions of different components of inactivation, we examined the relative amplitudes of each component and their voltage dependence. Fig. 8 shows the voltage dependence of fractional amplitudes of inactivation. There is one component of closed-state inactivation in the voltage range from −70 to −50 mV and two components at −40 mV. There are three components of open-state inactivation in the voltage range between −20 and +50 mV. Time constants for these different inactivation components are plotted in Figs. 1 and 6. The fast component of open-state inactivation was first seen at −30 mV, and its relative amplitude reached a saturating value of ~0.6 at −10 mV, where it dominated the inactivation process at voltages up to +50 mV (Fig. 8). The second, intermediate, component of open-state inactivation was largest at −30 mV, decreased as the depolarizing pulses become more positive and ultimately voltage insensitive between 0 and +50 mV. The third and slowest component was voltage insensitive in the range between −20 and +50 mV.

Our experiments performed on Kv4.3 indicate that the relative contribution of closed-state inactivation will depend on both time and voltage. The relative magnitude of the fast component of open-state inactivation becomes dominant as the depolarization pulses are positive to −20 mV. The contribution of closed-state inactivation is dominant in the voltage range from −50 to −70 mV. Hence, our data show that the relative contribution of closed-state versus open-state inactivation differs and depends on both the holding potential and the voltage amplitude of the depolarization pulse.

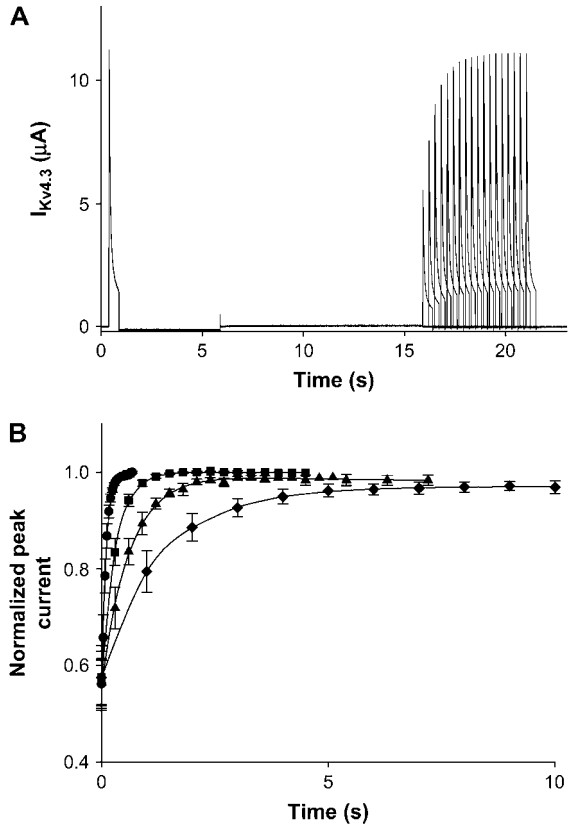

FIGURE 5 Voltage dependence of recovery from closed-state inactivation of $I_{Kv4.3}$. Voltage-clamp protocol consisted of five pulses: holding potential was −90 mV, first pulse (P1) amplitude is +50 mV and duration 500 ms, second pulse (P2) was set at −120 mV for 5000 ms, third pulse (P3) amplitude was −50 mV and duration 10,000 ms, the fourth pulse (P4) amplitude was varied from −120 to −70 mV and duration varied from 0 to 10,000 ms, and the fifth pulse (P5) was set at +50 mV for 500 ms. Panel *A* shows experimental current traces for P1–P5, with P4 = −80 mV. Normalized currents were plotted in panel *B* as a function of P4 duration (interpulse interval) at different voltages of P4: −120 mV (●, $n = 3$), −90 mV (■, $n = 5$), −80 mV (▲, $n = 6$), and −70 mV (♦, $n = 5$). Solid lines represent monoexponential fits to the experimental data for P4 voltages of −120 and −90 mV, and biexponential fits for P4 voltages of −80 and −70 mV.

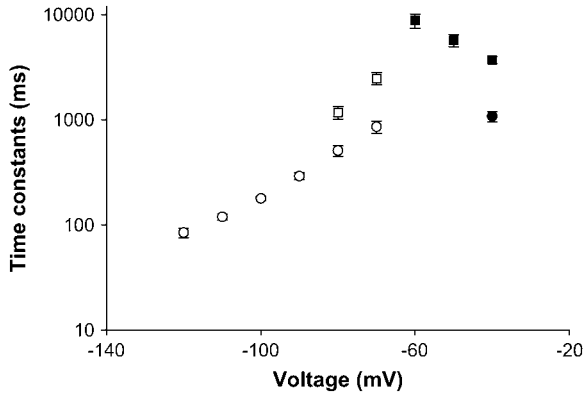

FIGURE 6 Kinetics of closed-state inactivation and recovery from closed-state inactivation. Data for closed-state inactivation ($n = 11$) and recovery from closed-state inactivation ($n = 6$) were shown by solid and open symbols, respectively. The protocols were the same as in Figs. 4 and 5. Circles and squares show fast and slow components.

Analysis of reopening (tail) currents

We have demonstrated the presence of three components of inactivation and proposed that inactivation proceeds predominantly from the open state when the holding potential is set at −90 mV and depolarizing potentials are positive to −30 mV. Inherent in the development of prior models of Kv4.3 gating was that inactivation of Kv4 occurred predominantly from the closed preopen state, resulting in accumulation in a closed-inactivated state after having transiently occupied an open-inactivated state (21,22). The latter transition, which includes recovery, would necessitate a series of transitions from the open-inactive state to the open state, the closed state and then the closed-inactive state. A previous study (22) considered decreasing reopening (tail) currents, with an increase in pulse duration, as a direct confirmation of their model of Kv4 gating. To estimate the time course of reopening currents, we used depolarizing pulses of different durations (from 64 to 964 ms) from the holding potential of −90 mV to +50 mV with subsequent repolarization to −120 mV at two concentrations $[K^+]_o = 98$ and 2 mM (Fig. 9, *A* and *B*). Extracellular $[K^+]$ of 98 mM was selected to maximize the K^+ electrochemical gradient and as a result the magnitude of the reopening current. At this $[K^+]_o$, the biexponential tail currents had a relatively large amplitude, which decreased in magnitude as pulse duration increased (Fig. 9 *A*). The initial component of reopening current (5–8 ms) was due to deactivation and could be partially obscured by the overlap with the capacitive transient. The slower second component was due to reopening of channels during recovery from inactivation. At 64 ms pulse duration, the time constants of the fast and slow components were 5.8 ± 1.1 and 34.8 ± 7.6 ms ($n = 4$), respectively, and normalized amplitudes for these two components were −0.81 ± 0.06 and −0.23 ± 0.04 ($n = 4$), respectively (current amplitudes were normalized to the value of the peak current during P1). At a longer pulse duration, 364 ms, the time constants of the fast and slow components were 3.0 ± 0.5 and 52.8 ± 11.6 ms ($n = 4$), respectively, and normalized amplitudes for these two components were −0.09 ± 0.02 and −0.16 ± 0.05 ($n = 4$), respectively. These data show that the increase in pulse duration led to a small decrease in the time constant of the first (fast) component, while the amplitude of this component decreased dramatically with pulse duration (Fig. 9). In addition, the increase in pulse duration led to an increase in the time constant of the second (slow) component, while the amplitude of the second component also decreased, but was less sensitive to pulse duration. To link these experiments to those performed at 2 mM $[K^+]_o$, we also measured reopening currents at 2 mM $[K^+]_o$ (Fig. 9 *B*). In general, the data appeared to be qualitatively similar to those observed at 98 mM

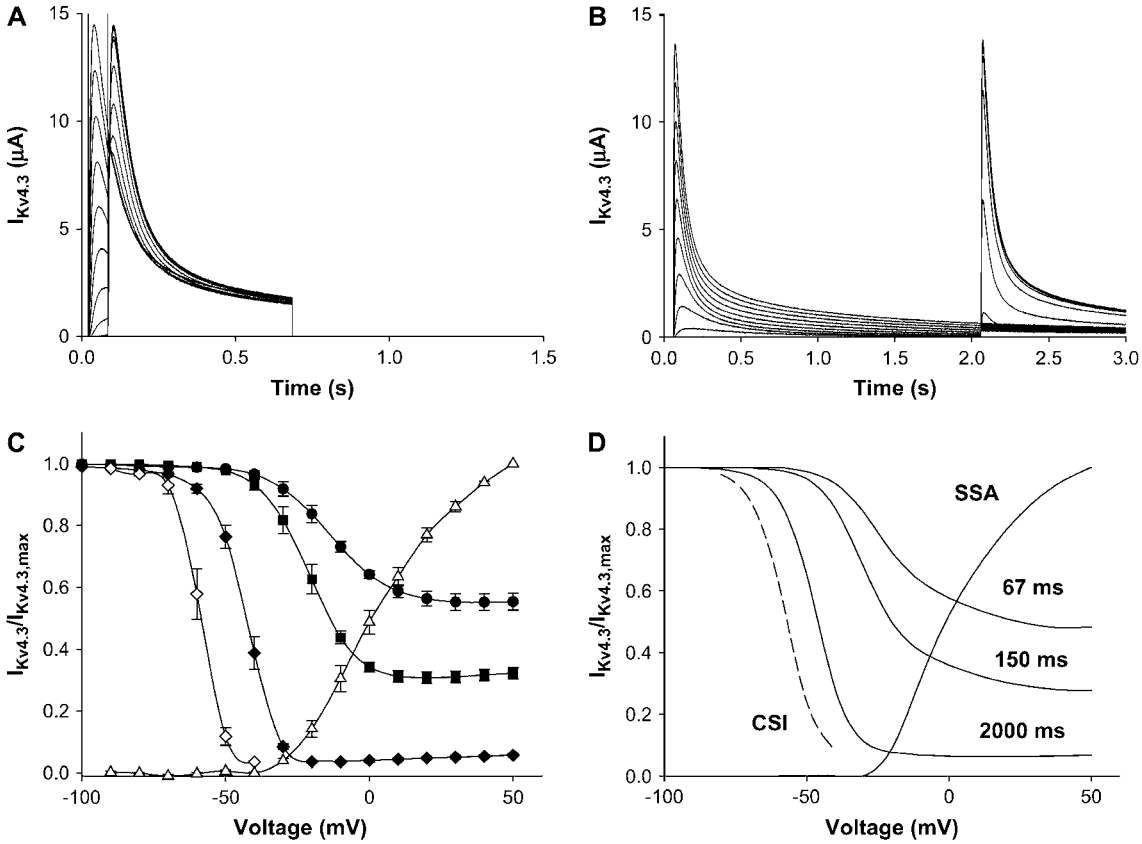

FIGURE 7 Isochronal inactivation as a function of voltage and pulse duration. Panels *A* and *B* show a series of current traces in response to either (*A*) 67- or (*B*) 2000-ms pulses (P1) from −120 to +50 mV applied from the holding potential −90 mV in 10-mV steps and followed by a second pulse (P2) to +50 mV. Panel *C* shows steady-state activation and isochronal inactivation relationships for 67 ms (●, $n = 5$), 150 ms (■, $n = 6$), and 2000 ms (*solid diamonds*, $n = 7$) P1 pulses for open-state inactivation. Data for closed-state inactivation are shown with ◇ ($n = 8$). Data for steady-state activation were plotted with △ (32) and fitted with function $f_a(V) = 1/\{1 + \exp[-(V - V_{1/2})/k]\}^4$. Fitting function for isochronal inactivation is $f_i(V) = f_{i0}/\{1 + \exp[(V - V_{1/2})/k]\} + (1 - f_{i0})$. Panel *D* shows the simulated steady-state activation (*SSA*), isochronal inactivation relationships for 67-, 150-, and 2000-ms pulses, and steady-state closed-state inactivation (*CSI*).

$[K^+]_o$, however, the small signal/noise ratio precluded extraction of values for the time constants and amplitudes for the two components. These experiments have been used as an alternate means of probing the recovery from inactivation pathway to complement those performed during the standard recovery from inactivation protocols shown in Fig. 2 and confirm the dependence of recovery on pulse duration (see next section).

Markov model and simulations of Kv4.3 inactivation

Review of our data on the kinetics of open- and closed-state inactivation and isochronal inactivation relationships led us to reexamine the Kv4.3 inactivation model (3). The existing model of Kv4.3 inactivation was based on the premise that Kv4 inactivation occurred predominantly from the closed preopen state (3). Open-state inactivation was deemed to result in a transient occupancy of the open-inactivated state. The reverse bias of the closed- to open-state transition led to an accumulation in a closed-inactivated state (3,21,22). Despite the success of these models in describing some of the gating properties of Kv4.x channels, analysis of simulations with the previously published Kv4.3 model (3) demonstrated marked inconsistencies with our experimental data for the kinetics of closed-state inactivation and isochronal inactivation relationships. In addition, a direct pathway between the open-inactivated and closed-inactivated states in previous models was not analyzed. For these reasons, we developed an 11-state Markov model that incorporated our previous experimentally based model of Kv4.3 activation (32), three open-inactivated and two closed-inactivated states, and included a direct connection between the open-inactivated and closed-inactivated states (Scheme 2). Our model is unique in that it includes direct transition between the third open-inactivated state and the closed-inactivated state.

In our model for Kv4.3 gating, the values of the rate constants in the activation pathway are the same as in our previously published model of Kv4.3 activation (32). The rate constants for the open to inactivated state transitions, for

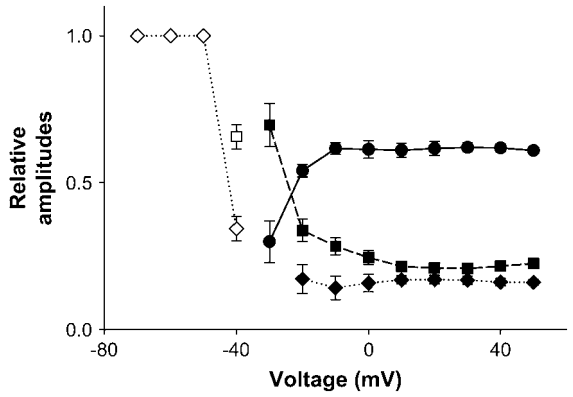

FIGURE 8 Voltage dependence of fractional amplitudes for open- and closed-state inactivation. Experimental data for closed- and open-state inactivation were plotted by open and solid symbols, respectively. Shown are amplitudes for the fast (●), intermediate (■), and slow (♦) components of open-state inactivation ($n = 6$). Open symbols (◇, □) show amplitudes of closed-state inactivation ($n = 11$).

the closed to inactivated state transitions, and the transitions between the inactivated states were derived from fitting the experimental data from open-state inactivation, closed-state inactivation, isochronal inactivation relationships, and recovery from inactivation, assuming thermodynamic reversibility. All these rate constants are voltage independent except for transitions between the two closed-inactivated states, I_{C3} and I_{C4} (Scheme 2). Numerical values for rate constants are presented in Table 3.

Figs. 1, 4, 7, and 9 show simulations using the different experimental protocols in this study. They reproduce the key features of the voltage and time dependence of inactivation in Kv4.3. The currents during 2000 ms depolarizing pulses display multiexponential kinetics that closely reproduce the experimental data (Fig. 1, *A* and *B*). In addition, the values of the time constants of simulated inactivation at different voltages compare well with the experimental data (Fig. 1, *C* and *D*). The model also closely reproduces the kinetics of closed-state inactivation, including biexponential kinetics at −40 mV (Fig. 4).

We were particularly interested in the time and voltage dependence of inactivation. Fig. 7 *D* shows simulations of isochronal inactivation relationships for depolarizing pulses of 67, 150, and 2000 ms duration. As can be seen, the simulations closely reproduce the experimental data on open- and closed-state inactivation (Fig. 7 *D*). Our experimental data predict that for short pulse durations the channel must open before open-state inactivation begins, which is simulated by our model (compare Fig. 7, *C* and *D*).

Our model also predicts decreasing reopening tail currents as depolarization pulse duration increases. This current has a biexponential time course, which represents deactivation and reopening of the channel resulting from partial recovery from open-state inactivation (Fig. 9 *C*). At 64 ms pulse duration, the time constants of the fast and slow components

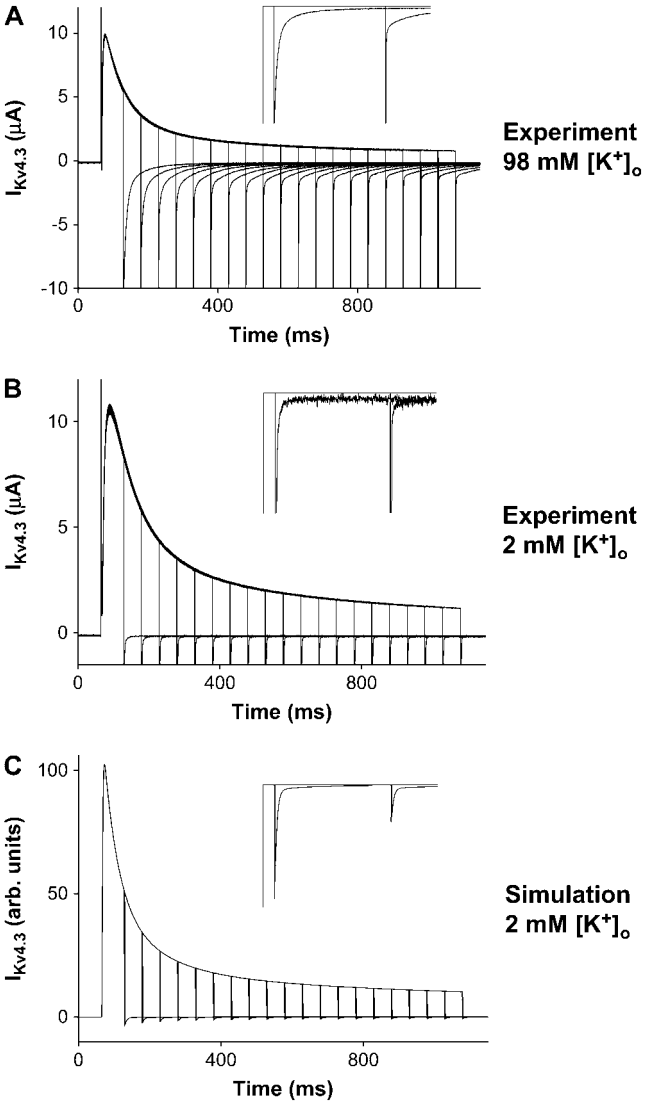

FIGURE 9 Reopening currents. Voltage-clamp protocol for the reopening currents consisted of two pulses: holding potential was −90 mV, first pulse (P1) amplitude is +50 mV and duration was variable; first pulse duration was set at 64 ms and the increments of subsequent pulses were set at 50 ms. The second pulse (P2) was set at −120 mV. Panels *A* and *B* show experimental reopening currents at two different extracellular $[K^+]$: 98 (*A*) and 2 mM (*B*). Panel *C* shows simulated reopening currents for extracellular $[K^+]$ of 2 mM. Inserts show magnified reopening currents induced by two P1 pulses with a 300 ms difference in duration. Panel *A* shows that the reopening currents at 98 mM $[K^+]_o$ are large in amplitude and had a biexponential time course. The amplitude of the first component decreases as a function P1 duration. Currents in panels *B* (experimental data) and *C* (simulations) at 2 mM $[K^+]_o$ are smaller, but show a similar time course.

were 5.2 and 82.9 ms, respectively, and normalized amplitudes for these two components were −0.03 and −0.002, respectively. At a longer pulse duration, 364 ms, the time constants of the fast and slow components were 5.2 and 104.4 ms, respectively, and normalized amplitudes for these two components were −0.01 and −0.001, respectively (current

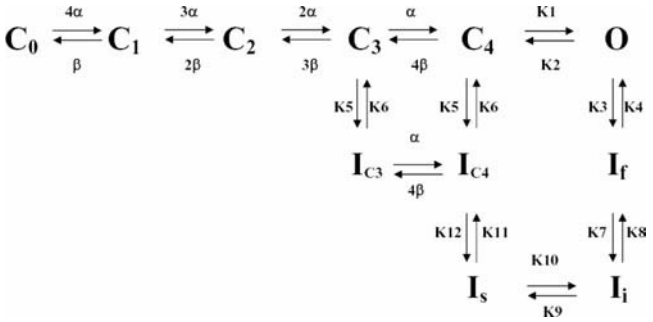

SCHEME 2

amplitudes were normalized to the value of the peak current during P1). The increase in pulse duration had no effect on the time constant of the first (fast) component, while the amplitude of this component decreased substantially with pulse duration. In addition, the increase in pulse duration led to an increase in the time constant of the second (slow) component. Although the amplitude of the second component also decreased, it was less sensitive to pulse duration. Our experimental and simulation data showed a similar time-dependent trend in the properties of both deactivation and reopening current (Fig. 9). On the other hand, differences were noted between the values of the amplitudes and time constants of the slow component (experimental versus simulated) and the amplitudes of the fast component of the reopening currents (experimental versus simulated). The latter difference is in part due to the differences in K^+ electrochemical gradient. Although these differences between the experimental and simulated data may reflect the limitations of our model in simulating recovery from inactivation, they must also reflect the effects of differences in $[K^+]_o$ on activation, deactivation, inactivation, and recovery. As a result, differences in experimental conditions only allow for a qualitative comparison between the two sets of data. Hence, one may conclude that these simulations are consistent with a recovery from inactivation that can proceed via both the open-inactivated to open transition as well as the direct open-inactivated to closed-inactivated transition (Scheme 2).

TABLE 3 Rate constants for Kv4.3 Markov model (Scheme 2)

$\alpha[V] = (1/(1 + \text{Exp}[(V + 10.0)/10.0]))*(0.425*\text{Exp}[0.27*V*0.03918]*\text{Exp}[(V + 10.0)/10.0] + 0.0836*\text{Exp}[0.83*V*0.03918])$.
$\beta[V] = (1/(1 + \text{Exp}[(V + 5.0)/10.0]))*(0.2244*\text{Exp}[-0.54*V*0.03918]*\text{Exp}[(V + 5.0)/10.0] + 0.0252*\text{Exp}[-0.48*V*0.03918])$.
$K1 = 6$
$K2 = 1.5$
$K3 = 0.021$
$K4 = 0.007$
$K5 = 0.0052$
$K6 = 0.000052$
$K7 = 0.0052$
$K8 = 0.0036$
$K9 = 0.0009$
$K10 = 0.04$
$K11 = 0.249941$
$K12 = 0.000975$
Rate constants are expressed as s^{-1}.

DISCUSSION

The cardiac transient outward K^+ current (I_{to}) plays a major role in the early part of repolarization. The contribution of I_{to} to repolarization is determined by the magnitude of the peak current and its rate of decay during the plateau of the action potential. Peak current is in part determined by open probability and inactivation. The decay of the transient outward K^+ current reflects inactivation of the K^+ channels. At fast heart rates, recovery from inactivation can be incomplete and results in cumulative inactivation. Hence, activation, inactivation, and recovery from inactivation of I_{to} play essential roles in determining the contribution of I_{to} to the cardiac action potential. Elucidation of the mechanisms of inactivation is essential for understanding the basis of cardiac repolarization.

Previous studies on Kv4.1, Kv4.2, and Kv4.3 (3,6,21,22) have indicated that inactivation can proceed from both the closed and open states of the channel, and that closed-state inactivation is of great importance. In fact, they concluded that closed-state inactivation is the predominant pathway of inactivation in Kv4 channels. In contrast, our data suggest that the different components of inactivation can be associated with different mechanisms and that open-state inactivation is the predominant pathway for inactivation during depolarizations positive to −30 mV. We show that Kv4.3 inactivation is a complex process that includes different voltage dependencies of open-, closed-state inactivation gating and recovery from inactivation. In particular, our observations demonstrated that inactivation and recovery from inactivation are also dependent on pulse duration, suggesting different coupling of inactivation to activation. Finally, we present a model for Kv4.3 gating that includes two separate inactivation pathways and closely simulated our experimental inactivation data.

We first examined macroscopic inactivation kinetics and found that they were voltage dependent and markedly different for closed- and open-state inactivation. Three time constants for open-state inactivation and two time constants for closed-state inactivation have been described in this article (Figs. 1 and 6) and by others (3,8,21,22). The kinetics of recovery from open-state inactivation also were strongly voltage dependent. They are monoexponential at very negative potentials and biexponential in the voltage range from −70 to −60 mV (Figs. 3 and 6). The use of short-, intermediate- and long-pulse protocols to evaluate isochronal inactivation and recovery enabled us to identify three separate inactivated states, with fast, intermediate, and slow time constants of inactivation. Significant differences in midpoint and slope of the isochronal inactivation relationships were observed. The implications of the existence of three distinct

inactivation pathways with different kinetic properties will be discussed below. Our observations argue against a previously published hypothesis that Kv4.3 inactivation primarily occurs from the closed state under all experimental conditions. We will now elaborate on each of these points.

It has been suggested that the mechanism of inactivation in Kv4 is distinct from that reported for *Shaker* K^+ channels, because the experiments on Kv4 inactivation did not fully recapitulate the principal findings reported for N- and C-type inactivation in *Shaker* (23–26). For example, the critical role played by the Kv4.2 N-terminus in generating the rapid component of Kv4.2 inactivation is confounded by the experiments that demonstrate that deletions of parts of the C-terminus in Kv4.1 and Kv4.3 also retard or remove the fast component of inactivation (20,34). The mechanisms underlying the intermediate and slow components are less clear. Hence, we examined in detail the fast, intermediate, and slow components of open-state inactivation to determine whether they represent three separate mechanisms and if so were they coupled in some way to activation?

Concepts about inactivation of K^+ channels have their roots in the classic Hodgkin-Huxley model, which treated inactivation of K^+ channels as a slow first-order process with voltage-dependent rate constants that are independent of the activation process. It is currently believed that inactivation of K^+ channels is dependent on activation, i.e., activation and inactivation are coupled (31,35,36). This dependence is predicted as gating transitions for activation represent conformational changes in the protein complex, that directly or indirectly (allosterically) affect other regions of the channel associated with inactivation (31). This view was strongly supported by the gating current measurements in K^+ channels (31,37–39), which showed that transient inactivation of K^+ channels was accompanied by a reduction in the size of the OFF gating currents and reflected charge immobilization (37,40–43). Charge immobilization indicates that activation does not reverse quickly once inactivation has occurred. Channels are locked in an ''activated form'' while inactivated and can deactivate fully once inactivation is removed through the recovery process.

To address the voltage dependence of the isochronal inactivation relationships for fast, intermediate, and slow components of open-state inactivation, we utilized three pulse durations of 67, 150, and 2000 ms (Fig. 7). Measurements of inactivation at the end of depolarization pulses with different voltages and durations to determine isochronal inactivation relationships assay the fraction of channels that have entered the inactivated states. The value of 67 ms was selected to minimize the contribution of slower inactivation pathways. On the other hand, the value of 150 ms was selected to achieve quasi-steady-state inactivation for the fast component, while recognizing that the intermediate component of inactivation would also make a contribution to inactivation during the 150 ms pulse. During the 2000 ms pulse, the fast and intermediate components of inactivation reached completion and the slow component nearly so. Appreciable differences were obtained for slope and midpoint of the isochronal inactivation relationships. A comparison of the $V_{1/2}$ of the steady-state isochronal inactivation relationships for 67 and 150, and 150 and 2000 ms pulses differed by 7.7 mV (−13.9 vs. −21.6 mV) and 21.8 mV (−21.6 vs. −43.4 mV). The values of k of the isochronal inactivation relationships for 67, 150, and 2000 ms are also different (10.3, 7.8, and 5.4 mV, respectively). They correspond to movement of different apparent effective charges 2.48 e_0, 3.27 e_0, and 4.72 e_0, respectively. Because values of $V_{1/2}$ of isochronal inactivation for the 67 and 150 ms pulses are more positive than the $V_{1/2}$ for steady-state activation (−29.4 mV) (32), we suggest that these two components of inactivation are coupled to activation (open state), i.e., these two components can only proceed after the channel opens.

We have used the term ''apparent effective charge'' throughout the manuscript to express the degree of voltage dependence in a consistent fashion. The apparent effective charge does not necessarily directly reflect charge movement associated with the inactivation process. Rather it reflects model-dependent properties of coupling to the activation process. The multiple overlapping components of inactivation complicate the separation of each state. As a result, each measurement contains some bias, such as the nonequilibrium problems associated with the interpretation of the isochronal inactivation relationships for various pulse durations. However, these measured charges are consistent with the analysis of the voltage dependence of amplitudes of fast, intermediate, and slow components, which if extrapolated to infinite time should be free of nonequilibrium artifacts. Taken in conjunction with the recovery data, a picture of channel inactivation emerges, in which time- and voltage-dependent properties are conferred by distinct inactivated states coupled to different states in the activation pathway.

The relatively large differences in estimated effective charge for inactivation may reflect discrete or abrupt transitions of individual channel subunits. One assumption that we made in the analysis of gating was that each of the four subunits operates independently and is an equal participant in the gating process. Evidence in support of this view is most clear in the case of activation. However, inactivation may instead result from the movement of fewer than four subunits. In this case, one could infer that the coordination of gating between individual subunits may not be necessary for all components of inactivation. On the other hand, the large range of values for estimated effective charge may instead reflect many small transitions within each of the subunits that are detected with the three widely different pulse durations. The relatively large number of domains in the Kv4.3 channel implicated in the inactivation process suggests that small conformational changes during inactivation can also be a basis for observed changes in gating characteristics.

How do the inactivation properties of Kv4.3 compare with N- and C-type inactivation seen in *Shaker* and Kv1.4? Kv1.4

was selected for comparison, because its N- and C-type inactivation properties share many similarities with *Shaker*. Comparison of inactivation variables, such as the values for $V_{1/2}$ and k for fast (N-type) and slow (C-type) inactivation in Kv1.4 demonstrates that the voltage dependence of N- and C-type inactivation in Kv1.4 is similar (18). The similarity in the voltage dependence of N- and C-type inactivation in Kv1.4 stands in marked contrast to the large differences in voltage dependence of isochronal inactivation properties of Kv4.3, supporting the view that the mechanism of inactivation in these two cases and their putative coupling to activation differ. In Kv1.4 the two types (N- and C-types) of inactivation are coupled to each other and had the same coupling to activation as was originally proposed for *Shaker* K^+ channels (25).

The disparity between the isochronal inactivation and the steady-state activation relationships may reflect different degrees of coupling to activation and/or voltage dependence of inactivation (Fig. 7). One interpretation of the differences in voltage dependence of open- (pulse durations of 67, 150, and 2000 ms) and closed-state inactivation is that their coupling to the activation process is different. The fast component is mediated by the binding of N-terminus (6), which is only possible after sufficient conformational changes during activation have made the binding site for the N-terminus accessible. The $V_{1/2}$ for the isochronal inactivation relationship during the 67 ms pulse at −13.9 mV is more positive than the $V_{1/2}$ of open-state activation relationship, −29.4 mV (32), and suggests that the fast component of inactivation appears to be coupled to an open state in the activation pathway. The $V_{1/2}$ of the closed-state inactivation relationship at −58.7 mV is more negative than that obtained for open-state activation and reflects coupling to a preopen closed state. In addition, the asymmetry of the steady-state activation relationship, conferred by the biexponential voltage dependence of activation kinetics (32), could account for the changes in k seen in the different isochronal relationships (for 67, 150, and 2000 ms pulses).

The interpretation of our data is influenced by a comparison with the inactivation data from Kv4.3, Kv4.2, and Kv4.1, where steady-state inactivation relationships were obtained by others using 5 s or longer prepulses (3,21,22). In studies performed by Jerng et al. (21), Bähring et al. (22), and Beck et al. (3), only relatively small differences in values of $V_{1/2}$ and k were noted. Comparison of these data indicates close agreement between their values of $V_{1/2}$ and k for steady-state inactivation (3,22) and our values obtained for closed-state inactivation. The use of 5-s or longer prepulses used in previous studies of steady-state inactivation (3,21,22) would have not allowed detection of isochronal inactivation relationships for fast and intermediate components of open-state inactivation.

Recovery from inactivation also can provide important insights into the gating of Kv4.3. Our data show a dependence of recovery from inactivation on pulse duration as well as voltage. The dependence of the recovery time constant on pulse duration can indicate overlap of several recovery pathways from different inactivated states. The relative contribution during recovery will be determined by the degree to which each of the particular components has contributed to inactivation. The fast component of inactivation has the largest contribution to inactivation of Kv4.3 (Fig. 8). Thus, the time constant of recovery from inactivation at negative potentials (−90 mV) after short pulse duration (67 ms) is monoexponential and mainly determined by recovery from the fast inactivated state (Fig. 2). We can expect the larger recovery time constants from the intermediate inactivated state. To test this hypothesis, we used a longer pulse duration (800 ms) and examined recovery from inactivation. We observed a larger time constant of recovery for the longer pulses (240 ± 6 vs. 179 ± 17 ms for long and short pulses at −90 mV, respectively), an effect that was also observed at −60 and −70 mV. This can be due to the relatively small contribution of recovery from intermediate inactive state (~20% of amplitude). The time constant of recovery from closed-state inactivation was even larger (296 ± 22 ms at −90 mV) (Fig. 5). Comparison of apparent effective charges for recovery obtained with different pulse duration shows an increase in their values (0.77 e_0, 0.94 e_0, and 1.20 e_0 for short- and long-pulse recovery from open state, and recovery from closed-state inactivation, respectively). We suggest that this reflects different coupling of recovery to the deactivation process. The voltage dependence of recovery rate indicates that inactivation is terminated by the backward movement of S4 enabling recovery from inactivation to proceed. This view is supported by the similarity of values between the apparent effective charge for recovery from inactivation and deactivation (0.48 e_0) (32).

Thus, the differences in voltage dependence of the open-state isochronal inactivation relationships elicited by different pulses (67, 150, and 2000 ms pulses), the differences in recovery kinetics elicited by pulses with different durations (67 and 800 ms), the voltage dependence of relative current amplitude in conjunction with three different time constants of inactivation strongly support the existence of multiple open-state inactivation pathways for Kv4.3.

Simulations

Our model of Kv4.3 gating, which is based on two pathways of inactivation, closely simulates the different components of inactivation kinetics throughout a wide range of voltages, the voltage dependence of inactivation, the voltage dependence of closed-state inactivation, the isochronal inactivation relationships, and the reopening currents. The isochronal inactivation relationships, with different pulse durations (67–2000 ms), result in different fractions of Kv4.3 channels that are in the different inactivated states at the end of each pulse. These differences would provide us with another avenue for assessing the ability of our model to simulate inactivation and its coupling

to activation. As we showed the simulations reproduce the experimental data (Fig. 7, *C* and *D*). Our model predicts the shifts in $V_{1/2}$ and change in k for isochronal inactivation relationships for the changes in pulse duration. It is of interest that our model predicts a predominant role of open-state inactivation at depolarizations positive to −30 mV. At relatively short depolarization pulse 67 ms, the $V_{1/2}$ of isochronal inactivation relationship is close to the value of $V_{1/2}$ for steady-state activation (Fig. 7 *D*). This implies that in this voltage range the channel is in the open state before it inactivates.

Although our model closely simulates our experimental data, one set of experiments appears to oppose the foundation of this model. In a recent report, Shahidullah and Covarrubias (28) have shown that Rb^+ slows the rates of Kv4.3 deactivation and inactivation. Because Rb^+ increases the mean open time, favoring the open state, the slowing of deactivation supports the conclusion that inactivation is mainly coupled to a closed (preopen) state. Their interpretation of the experimental data is based on a model, where inactivation of Kv4.3 occurs predominantly via the preopen closed state. We suggest that the increase in opening time and decrease in deactivation and inactivation rates reflect a deepening of the energy minimum for the open conformation of Kv4.3. In this case, Kv4.3 has to overcome a larger barrier during transitions from the open to closed states as well as from the open to open-inactivated state, provided that the energy minima for the closed and inactivated states are not affected substantially. In other words, Rb^+ does not simply produce a voltage shift in gating, but slows the rates for the two pathways that lead from the open state. The indirect evidence supporting our interpretation is that the Rb^+ also slows the rate of activation (see Fig. 5 in Shahidullah and Covarrubias (28)), an effect that does not simply follow from the negative shift of voltage dependence of G/G_{max} in Rb^+.

In addition to closely reproducing different aspects of Kv4.3 inactivation, we reproduced recovery from inactivation at −70 mV. At this potential we were able to simulate both the biexponential recovery from inactivation for both long and short pulses as well as the values of the time constants for recovery. Despite the successful reproduction of inactivation data, this model could not simulate the voltage dependence of recovery from inactivation. Attempts to overcome this limitation by incorporating an additional closed-inactivated state along with a voltage-dependent transition between I_S and I_{C3} were unsuccessful. This limitation is common to the other gating model of Kv4.3 (3). This suggests that the models do not incorporate adequate energetic coupling to the deactivation process to fully simulate the experimental data.

Physiological implications

We have demonstrated that pulse duration during voltage-clamp experiments is an important determinant of the inactivation process, an observation that has important physiological implications. Pulses of 150 ms only induced rapid and intermediate components of inactivation. The values of 67 and 150 ms would correspond to the action potential duration of an atrial cell and to the duration of the plateau in a ventricular myocyte, respectively. These data have implications for the different degrees of cumulative inactivation of I_{to} during the repetitive sequence of atrial and ventricular action potentials. We wish to emphasize that experimental conditions also will determine the relative contribution of open-state and/or closed-state inactivation to the inactivation of Kv4.3. The determination of which pathway is preferentially selected will be dependent on the voltage and time. In cardiac myocytes, which have resting potentials between −90 and −85 mV under physiological $[K^+]_o$, a transient (<100 ms) depolarization to +30 mV will result in open-state inactivation. On the other hand, under conditions of acute myocardial ischemia, when extracellular $[K^+]_o$ has been reported to rise to 10–12 mM, resting potential would be expected to be ~−65 mV, where closed-state inactivation would become appreciable (44). In neurons, potentials between rapid depolarizations are considerably more positive than in cardiac myocytes leading to a greater degree of closed-state inactivation under physiological conditions.

APPENDIX

Voltage dependence for time constant of inactivation

Inactivation can show voltage dependence in two ways, intrinsic voltage dependence or through its coupling to S4 movement and activation.

To understand how voltage-dependent time constants of inactivation can develop, consider the simple Markov model of channel gating:

$$\mathrm{C} \underset{\beta(V)}{\overset{\alpha(V)}{\longleftrightarrow}} \mathrm{O} \underset{k_b}{\overset{k_f}{\longleftrightarrow}} \mathrm{I}, \tag{1}$$

where $\alpha(V)$ and $\beta(V)$ are the voltage-dependent activation and deactivation rates, respectively, k_f and k_b are the voltage-independent forward and backward inactivation rates, respectively, and C, O, and I are the closed, open, and inactivated states, respectively.

In the absence of inactivation, the equilibrium open probability (P_O) is

$$P_O = \frac{1}{1 + \exp[-z_a e_0 (V - V_{1/2})/k_B T]}, \tag{2}$$

where z_a is the activation gating charge. The ratio of probability of the channels to be in the open and closed states at equilibrium is

$$\frac{P_O}{P_C} = \exp[z_a e_0 (V - V_{1/2})/k_B T]. \tag{3}$$

When the membrane is rapidly depolarized to very positive potentials, P_O rapidly approaches 1 and the time course of development of inactivation proceeds with a time constant of

$$\tau_i = \frac{1}{k_f + k_b}. \tag{4}$$

In many cases of interest including Kv4.3

$$k_f \gg k_b\,, \tag{5}$$

and as a result we can make the approximation

$$\tau_i \approx \frac{1}{k_f}. \tag{6}$$

Our system can, therefore, be simplified to

$$C \underset{\beta(V)}{\overset{\alpha(V)}{\longleftrightarrow}} O \xrightarrow{k_f} I, \tag{7}$$

and the probability of the channel to be in the inactivated state can be expressed as a differential equation:

$$\frac{dP_I}{dt} = -k_f P_O. \tag{8}$$

Assuming that activation is much faster than inactivation, P_O should be always proportional to P_C according to the relationship

$$\frac{P_O}{P_C} = \exp[z_a e_0 (V - V_{1/2})/k_B T], \tag{9}$$

or

$$P_C = P_O \exp[-z_a e_0 (V - V_{1/2})/k_B T]. \tag{10}$$

The last equation yields from mass balance

$$P_O = 1 - P_C - P_I = 1 - P_O \exp[-z_a e_0 (V - V_{1/2})/k_B T] - P_I. \tag{11}$$

Substituting Eq. 11 into Eq. 8 yields

$$\begin{aligned}\frac{dP_I}{dt} &= \frac{-k_f (1 - P_I)}{1 + \exp[-z_a e_0 (V - V_{1/2})/k_B T]} \\ &= -\frac{k_f}{1 + \exp[-z_a e_0 (V - V_{1/2})/k_B T]} \\ &\quad + \frac{k_f P_I}{1 + \exp[-z_a e_0 (V - V_{1/2})/k_B T]},\end{aligned} \tag{12}$$

which has a solution with a time constant (τ_i)

$$\tau_i = k_f^{-1}\{1 + \exp[-z_a e_0 (V - V_{1/2})/k_B T]\}. \tag{13}$$

An apparent effective charge can be calculated from Eq. 13 that has a direct relationship to the equivalent charge for the activation to which the inactivation process is coupled.

Effective charge and equilibrium

The steep voltage dependence of steady-state inactivation observed in many channels comes from a coupling to activation. In the simple Markov model for channel gating:

$$C \underset{\beta(V)}{\overset{\alpha(V)}{\longleftrightarrow}} O \underset{k_b}{\overset{k_f}{\longleftrightarrow}} I\,, \tag{14}$$

steady-state activation in the absence of inactivation can be described by equation

$$\frac{1}{1+\exp[-z_a e_0 (V - V_{1/2})/k_B T]}. \tag{15}$$

The ratio between P_C and P_O at equilibrium is always described by Eq. 9. Similarly, with inactivation the ratio between P_O and P_I is given by

$$\frac{P_O}{P_I} = \frac{k_b}{k_f}. \tag{16}$$

The ratio of P_I/P_C is equal to

$$\frac{P_I}{P_C} = \frac{P_O/P_C}{P_O/P_I} = \frac{k_f}{k_b} \exp[z_a e_0 (V - V_{1/2})/k_B T]\,, \tag{17}$$

and results in an equilibrium dependence of

$$P_I = \frac{1}{1 + k_b/k_f} \times \frac{1}{1 + \frac{k_f}{k_b} \exp[-z_a e_0 (V - V_{1/2})/k_B T]}, \tag{18}$$

or as a simple addition of free energy that stabilizes the inactivated state. This would also tend to shift the $V_{1/2}$ for inactivation to the left of that for activation, but the apparent charge determined from steady-state or isochronal inactivation relationship should still reflect the equivalent gating charge for steady-state activation of the activated state(s) to which a particular inactivation process is coupled.

Effective charge of recovery

Early work on single Na^+ channels (31,45) observed that the development of inactivation was intrinsically voltage insensitive in the forward direction, after activation. However, recovery from inactivation was an intrinsically voltage-sensitive process. In a simple model of coupling

$$C \underset{\beta(V)}{\overset{\alpha(V)}{\longleftrightarrow}} O \underset{k_b}{\overset{k_f}{\longleftrightarrow}} I\,, \tag{19}$$

the backwards rate for recovery will be limited by k_b at hyperpolarized potentials. Voltage dependence for the recovery from inactivation could be obtained by allowing backwards movement of the voltage sensor to destabilize the inactivation process (31,43,45). Kinetically this might be described as

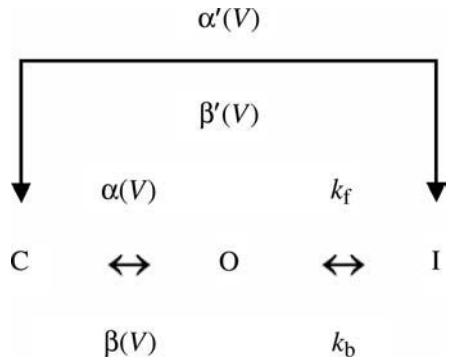

(20)

where α' and β' have the same net equivalent charge as α and β to preserve thermodynamic reversibility (46). The steepness of the voltage dependence of recovery rate, therefore, is unlike the effective charge of inactivation rate and equilibrium. It does not reflect the probability of the open state or states to which inactivation is coupled, but instead reflects the voltage dependence of a limited set of transitions near but below the inactivation coupling threshold. However, it is clear that inactivated states that are coupled to different states of the activation pathway are likely to show different voltage dependencies of the recovery (effective charge of recovery).

This work was supported in part by National Heart, Lung, and Blood Institute grants 19216, 52874, and 62465, the National Science Foundation

KDI-DBI-9873173, a grant from the American Heart Association, and a grant from the Oishei Foundation.

REFERENCES

1. Campbell, D. L., R. L. Rasmusson, M. B. Comer, and H. C. Strauss. 1995. The cardiac calcium-independent transient outward potassium current: kinetics, molecular properties, and role in ventricular repolarization. *In* Cardiac Electrophysiology: From Cell to Bedside, 2nd Ed. D. Zipes and J. Jalife, editors. WB Saunders, Philadelphia, PA. 83–96.
2. Strauss, H. C., M. J. Morales, S. Wang, M. V. Brahmajothi, and D. L. Campbell. 2001. Voltage dependent K^+ channels. *In* Heart Physiology and Pathophysiology, 4th Ed. N. Sperelakis, Y. Kurachi, A. Terzic, and M. V. Cohen, editors. Academic Press, San Diego, CA. 259–280.
3. Beck, E. J., M. Bowlby, W. F. An, K. J. Rhodes, and M. Covarrubias. 2002. Remodelling inactivation gating of Kv4 channels by KChIP1, a small-molecular-weight calcium-binding protein. *J. Physiol.* 538: 691–706.
4. Amberg, G. C., S. D. Koh, Y. Imaizumi, S. Ohya, and K. M. Sanders. 2003. A-type potassium currents in smooth muscle. *Am. J. Physiol.* 284:C583–C595.
5. Birnbaum, S. G., A. W. Varga, L. L. Yuan, A. E. Anderson, J. D. Sweatt, and L. A. Schrader. 2004. Structure and function of Kv4-family transient potassium channels. *Physiol. Rev.* 84:803–833.
6. Gebauer, M., D. Isbrandt, K. Sauter, B. Callsen, A. Nolting, O. Pongs, and R. Bähring. 2004. N-type inactivation features of Kv4.2 channel gating. *Biophys. J.* 86:210–223.
7. Jerng, H. H., P. J. Pfaffinger, and M. Covarrubias. 2004. Molecular physiology and modulation of somatodendritic A-type potassium channels. *Mol. Cell. Neurosci.* 27:343–369.
8. Patel, S. P., R. Parai, R. Parai, and D. L. Campbell. 2004. Regulation of Kv4.3 voltage-dependent gating kinetics by KChIP2 isoforms. *J. Physiol.* 557:19–41.
9. Patel, S. P., and D. L. Campbell. 2005. Transient outward potassium current, ''Ito'', phenotypes in the mammalian left ventricle: underlying molecular, cellular and biophysical mechanisms. *J. Physiol.* Apr14. [Epub ahead of print].
10. Muraki, K., Y. Imaizumi, M. Watanabe, Y. Habuchi, and W. R. Giles. 1995. Delayed rectifier K^+ current in rabbit atrial myocytes. *Am. J. Physiol.* 269:H524–H532.
11. Sah, R., R. J. Ramirez, G. Y. Oudit, D. Gidrewicz, M. G. Trivieri, C. Zobel, and P. H. Backx. 2003. Regulation of cardiac excitation-contraction coupling by action potential repolarization: role of the transient outward potassium current (I_{to}). *J. Physiol.* 546:5–18.
12. Dixon, J. E., W. Shi, H. S. Wang, C. McDonald, H. Yu, R. S. Wymore, I. S. Cohen, and D. McKinnon. 1996. Role of the Kv4.3 K^+ channel in ventricular muscle. A molecular correlate for the transient outward current. *Circ. Res.* 79:659–668.
13. Yeola, S. W., and D. J. Snyders. 1997. Electrophysiological and pharmacological correspondence between Kv4.2 current and rat cardiac transient outward current. *Cardiovasc. Res.* 33:540–547.
14. Brahmajothi, M. V., D. L. Campbell, R. L. Rasmusson, M. J. Morales, J. S. Trimmer, J. M. Nerbonne, and H. C. Strauss. 1999. Distinct transient outward potassium current (I_{to}) phenotypes and distribution of fast-inactivating potassium channel alpha subunits in ferret left ventricular myocytes. *J. Gen. Physiol.* 113:581–600.
15. Nerbonne, J. M. 2000. Molecular basis of functional voltage-gated K^+ channel diversity in the mammalian myocardium. *J. Physiol.* 525:285–298.
16. Nerbonne, J. M., C. G. Nichols, and T. L. Schwarz. 2001. Genetic manipulation of a cardiac K^+ channel function in mice. What have we learned and where do we go from here? *Circ. Res.* 89:944–956.
17. Radicke, S., D. Cotella, E. M. Graf, U. Ravens, and E. Wettwer. 2005. Expression and function of dipeptidyl-aminopeptidase-like protein 6 as a putative β-subunit of human cardiac transient outward current encoded by Kv4.3. *J. Physiol.* 565:751–756.
18. Rasmusson, R. L., M. J. Morales, R. C. Castellino, Y. Zhang, D. L. Campbell, and H. C. Strauss. 1995. C-type inactivation controls recovery in a fast inactivating cardiac K^+ channel (Kv1.4) expressed in *Xenopus* oocytes. *J. Physiol.* 489:709–721.
19. Liu, Y., M. E. Jurman, and G. Yellen. 1996. Dynamic rearrangement of the outer mouth of a K^+ channel during gating. *Neuron.* 16:859–867.
20. Jerng, H. H., and M. Covarrubias. 1997. K^+ channel inactivation mediated by the concerted action of the cytoplasmic N- and C-terminal domains. *Biophys. J.* 72:163–174.
21. Jerng, H. H., M. Shahidullah, and M. Covarurubias. 1999. Inactivation gating of Kv4 potassium channels. Molecular interactions involving the inner vestibule of the pore. *J. Gen. Physiol.* 113:641–659.
22. Bähring, R., L. M. Boland, A. Varghese, M. Gebauer, and O. Pongs. 2001. Kinetic analysis of open- and closed-state inactivation transitions in human Kv4.2 A-type potassium channels. *J. Physiol.* 535:65–81.
23. Zagotta, W. N., T. Hoshi, and R. W. Aldrich. 1990. Restoration of inactivation in mutants of *Shaker* potassium channels by a peptide derived from ShB. *Science.* 250:568–571.
24. Hoshi, T., W. N. Zagotta, and R. W. Aldrich. 1991. Two types of inactivation in Shaker K^+ channels: effects of alterations in the carboxy-terminal region. *Neuron.* 7:547–556.
25. Baukrowitz, T., and G. Yellen. 1995. Modulation of K^+ current by frequency and external $[K^+]$: a tale of two inactivation mechanisms. *Neuron.* 15:951–960.
26. Rasmusson, R. L., M. J. Morales, S. Wang, S. Liu, D. L. Campbell, M. V. Brahmajothi, and H. C. Strauss. 1998. Inactivation of voltage-gated cardiac K^+ channels. *Circ. Res.* 82:739–750.
27. Jiang, X., G. C. L. Bett, X. Li, V. E. Bondarenko, and R. L. Rasmusson. 2003. C-type inactivation involves a significant decrease in the intracellular aqueous pore volume of Kv1.4 K^+ channels expressed in Xenopus oocytes. *J. Physiol.* 549:683–695.
28. Shahidullah, M., and M. Covarrubias. 2003. The link between ion permeation and inactivation gating of Kv4 potassium channels. *Biophys. J.* 84:928–941.
29. Wang, S., S. P. Patel, Y. Qu, P. Hua, H. C. Strauss, and M. J. Morales. 2002. Kinetic properties of Kv4.3 and their modulation by KChIP2b. *Biochem. Biophys. Res. Commun.* 295:223–229.
30. Comer, M. B., D. L. Campbell, R. L. Rasmusson, D. R. Lamson, M. J. Morales, Y. Zhang, and H. C. Strauss. 1994. Cloning and characterization of an I_{to}-like potassium channel from ferret ventricle. *Am. J. Physiol.* 267:H1383–H1395.
31. Hille, B. 2001. Ion Channels of Excitable Membranes, 3rd Ed. Sinauer Associates, Sunderland, MA.
32. Wang, S., V. E. Bondarenko, Y. Qu, M. J. Morales, R. L. Rasmusson, and H. C. Strauss. 2004. Activation properties of Kv4.3 channels: time, voltage and $[K^+]_o$ dependence. *J. Physiol.* 557:705–717.
33. Beck, E. J., and M. Covarrubias. 2001. Kv4 channels exhibit modulation of closed-state inactivation in inside-out patches. *Biophys. J.* 81:867–883.
34. Hatano, H., S. Ohya, K. Muraki, R. B. Clark, and W. R. Giles. 2004. Two arginines in the cytoplasmic C-terminal domain are essential for voltage-dependent regulation of A-type K^+ current in the Kv4 channel subfamily. *J. Biol. Chem.* 279:5450–5459.
35. Armstrong, C. M. 1981. Sodium channels and gating currents. *Physiol. Rev.* 61:644–683.
36. Bezanilla, F. 2000. The voltage sensor in voltage-dependent ion channels. *Physiol. Rev.* 80:555–592.
37. Bezanilla, F., E. Perozo, D. M. Papazian, and E. Stefani. 1991. Molecular basis of gating charge immobilization in *Shaker* potassium channels. *Science.* 254:679–683.

38. Perozo, E., D. M. Papazian, E. Stefani, and F. Bezanilla. 1992. Gating currents in *Shaker* K^+ channels. Implications for activation and inactivation models. *Biophys. J.* 62:160–168.

39. Perozo, E. 2002. New structural perspectives on K^+ channel gating. *Structure* (*Camb.*). 10:1027–1029.

40. Armstrong, C. M., and F. Bezanilla. 1977. Inactivation of the sodium channel. II. Gating current experiments. *J. Gen. Physiol.* 70:567–590.

41. Stimers, J. R., F. Bezanilla, and R. E. Taylor. 1985. Sodium channel activation in the squid gain axon. Steady state properties. *J. Gen. Physiol.* 85:65–82.

42. Vandenberg, C. A., and F. Bezanilla. 1991. A sodium channel gating model based on single channel, macroscopic ionic and gating currents in the squid giant axon. *Biophys. J.* 60:1511–1533.

43. Patlak, J. B. 1991. Molecular kinetics of the voltage-dependent Na^+ channel. *Physiol. Rev.* 71:1047–1080.

44. Owens, L. M., T. A. Fralix, E. Murphy, W. E. Cascio, and L. S. Gettes. 1996. Correlation of ischemia-induced extracellular and intracellular ion changes to cell-to-cell electrical uncoupling in isolated blood-perfused rabbit hearts. Experimental Working Group. *Circulation.* 94:10–13.

45. Aldrich, R. W., D. P. Corey, and C. F. Stevens. 1983. A reinterpretation of mammalian sodium channel gating based on single channel recording. *Nature.* 306:436–441.

46. Labarca, P., R. Coronado, and C. Miller. 1980. Thermodynamic and kinetic studies of the gating behavior of a K^+-selective channel from the sarcoplasmic reticulum membrane. *J. Gen. Physiol.* 76:397–424.